

Two-Port Silicon-Based MIMO Nano-Dielectric Resonator Antenna with Polarization Diversity for Photonics Applications

Shailza Gotra^{1, *} and Vinay S. Pandey²

Abstract—This paper demonstrates a compact two-port multi-input multi-output optical nano-antenna with polarization diversity. The proposed antenna consists of a silicon-based radiating element that explores the possibilities of using a highly efficient dielectric resonator over the conventional metallic antennas at THz regime. The specific position of the Gaussian pulse excitation generates the 90° phase difference between the field components travelling across the edges of silver nanostrip feedlines. This generates the orthogonal field components which results in the achievement of circular polarization. Furthermore, any deviation in the excitation position at the port disturbs the field components resulting in linear polarization. This approach provides the polarization diversity using different excitation positions at ports. Considering the analytical stage of this proposed work, the detailed design guidelines and analysis are also discussed. The antenna provides circularly polarized radiations having 6.78% of 3 dB axial-ratio bandwidth and linearly polarized response using the optimized feeding positions at the respective ports for obtaining the polarization diversity performance. The isolation of more than 15 dB is maintained between the ports over the entire operating passband of the antenna. The proposed antenna with the optimized dimensions can be utilized for the optical C- and L-band applications.

1. INTRODUCTION

The optical nano-antenna excites the specific local modes into the far-field optical radiations of the photonics-based nanostructures and vice-versa [1]. In the present scenario, the miniaturization of the system is highly demanding. Thus, on-chip communication technologies have been adopted at a faster pace [2]. The scintillating performance of optical nanoscale antennas has secured attention through various studies [3–5]. These studies focus on the impedance matching and coupling efficiency of optical antennas [6, 7], excitation of plasmonic waveguides [8], and tapered transmission lines [9] using nano-antennas. Optical antennas have gained attention in the detection of light frequency signals. These antennas emerge as the potential competitor of conventional semiconductor based photodetectors because of their comparatively easy installation, cost effectiveness, and suitable detection of signals [10]. According to ITU standards, optical C-band (1550 nm) offers suitable long-haul transmission. Optical antennas offer the miniaturization of conventional antennas by adopting similar designing and analytical approach [11]. This leads to the development in the field of nanotechnology by reducing the size of the nano-networks effectively. Nano-antennas have been widely reported with various applications in solar cells, optoelectronics, networking on-chip devices, and spectroscopy [12]. A preliminary study on an array configuration of rectified optical nano-antennas was reported for energy harvesting application [13]. These antennas use electromagnetic simulators for numerical and theoretical analysis. Consequently, this field requires the development in the field of communication with the perspective of fabrication and

Received 11 November 2022, Accepted 3 February 2023, Scheduled 7 February 2023

* Corresponding author: Shailza Gotra (shailzagotra@outlook.com).

¹ Department of Electronics and Communication Engineering, Indian Institute of Technology Roorkee, India. ² Department of Applied Sciences, National Institute of Technology Delhi, India.

measurement. This will make the prominent advancement in the field of nanotechnology by designing optical nano-antennas.

At radio frequency ranges, metallic antennas play a vital role in antenna designing. However, these antennas experience the inherent conduction losses at microwave and millimetre wave applications. At higher frequency ranges, metals do not follow the ideal conducting properties due to which a replacement of conducting material is highly required for the development in the optical regime [14]. To overcome this limitation, the use of a dielectric resonator as the main radiating element has gained the spotlight. Dielectric resonator antenna (DRA) has been extensively studied due to its attracting features like wide bandwidth, high radiation efficiency, high gain, low profile, and low surface and conduction losses over the conventional conducting antennas [15]. Also, DR allows the exposition of various modes using appropriate excitation technique [16–18]. These exhibit modes inside the resonator predict the radiation pattern and far-field parametric behaviour of the antenna. These features snatch the attention of researchers in the field of antenna designing. Mostly, the radiating element consists of the ceramic-based dielectric material having relative permittivity varying in the range 10–100 at microwave frequency ranges [15]. However, ceramic material is inefficient to be used in THz band applications. To overcome this limitation, silicon-based antennas provide low losses while being integrated with the active elements for on-chip applications. Silicon provides the promising characteristics due to the high resistivity and stable permittivity at the millimetre wave and THz applications as reported in [19]. In [20], a dielectric resonator reflectarray using silicon material at THz frequency was reported. Based on the above-mentioned features of the silicon, it can be considered as a prominent transparent material at the optical regime for photonics applications [21–23]. Notably, most nano-antennas were reported with the linearly polarized (LP) response in the operating passband. However, at higher frequency ranges, the compactness of the transceiver limits the control of the misalignment losses at nanoscale. This can be overcome by using circularly polarized (CP) antennas [24]. The modelling of photonics and optical devices requires the rigorous analysis of wave polarization and its manipulation for the electromagnetic signal processing. In this manner, the approach of using anisotropic materials or meta-structures was reported as an alternative way to control the polarization of the radiating wave. The polarization phenomenon in optical devices carries the continuous information package, thus, its manipulation is one of the prominent tasks. In [25], the in-plane anisotropy of the black phosphorous material was utilized for controlling the polarization state. The investigation involved the filtering of electromagnetic fields for the rotation of polarization axis (LP to CP conversion). The detailed study on the exploration of several plasmonic materials based meta-structures was reported in [26]. This reported work utilized the two metallo-dielectric stacks optimization with the objective of achieving the multiple polarizations. The literature shows a very few CP nano-antennas reported at millimetre wave and THz frequency ranges. A nano-ring slot antenna with CP response was reported for uniform overheating applications like treating cancer tumour [27]. Regardless of all the techniques adopted at microwave frequency [28], achieving the CP response at optical regime is still under investigation.

With the advancement in wireless communication, multi-input-multi-output (MIMO) technology has been widely used for achieving higher data rate as the signal power level and bandwidth are the limited constraints [29]. The optical regime has offered the virtual unregulated bandwidth worldwide with security that encourages the development in nanotechnology. A study on optical MIMO was reported using zero forcing technique. The reported study achieved the multiplexing and higher data transmission rate by setting multiple transmitting and receiving optical antennas [30]. Also, a photonics-based MIMO radar architecture was reported using optical transceivers [31]. However, the design of MIMO antennas with the achievement of polarization diversity remains to be addressed in the literature. Hence, several concerns in the field of optical antenna designing need focus on designing a MIMO configuration including polarization control analysis.

In this regard, a silicon-based rectangular two-port CP MIMO nano-DRA is proposed with the circular polarization generation technique using specific feeding mechanism. A technique is implemented to obtain the polarization diversity using different excitation positions at the ports. The isolation between the ports has been maintained due to the generation of orthogonal degenerate modes. The proposed nano-DRA with selected dimensions can be used for various optical L- and C-band applications like optical magnetic recording, near field scanning, optical microscopy, and optical wireless interconnects which requires CP radiations [32]. The architecture of this paper consists of the antenna

geometry explained in Section 2, followed by the design guidelines and analysis explained in Section 3. The results and discussion and parametric analysis are explained in Sections 4 and 5, respectively. Later, Section 6 includes the conclusion of this work.

2. ANTENNA GEOMETRY

Figure 1 shows the proposed antenna geometry of the two-port MIMO nano-DRA. The geometry consists of two substrate layers having dimensions $l_s \times w_s$ and height h_1 and h_3 , respectively and placed above the ground plane. The substrate is made up of silicon dioxide (SiO_2) material having relative permittivity, $\epsilon_s = 2.1$. The proposed DR is excited by the input Gaussian pulse using two nanostrip feedlines made up of silver (Ag) material having dimensions $l_f \times w_f$ with stub length, s . The dispersive properties of Ag are analysed using Drude’s model [33]. A thin film of silver having height h_2 is deposited over the substrate to form a feedline structure. The nanostrip feedlines are inserted within the two substrate layers following the gap, g , between them. The separation between the feedlines is maintained by inserting the SiO_2 substrate material. The substrate layer having thickness h_3 is put on top to separate the direct contact between the DR and metallic feedline. This type of feeding arrangement follows the mechanism of proximity coupled feeding. This provides improved matching and wide impedance bandwidth. The rectangular DR made up of silicon (Si) material having dimensions $a \times b \times h$ with relative permittivity $\epsilon_r = 11.56$ is placed above the substrate layers. From the fabrication perspective, the experimental realization of the prototype requires unconventional microfabrication approach with the advanced process of single crystal layers bonding, photolithography, and deep reactive ion etching. The detailed fabrication procedure of the silicon-based terahertz DRA was reported in [34]. Further, the characterization of the fabricated samples and experimental validation of the results requires dedicated equipment and measurement setup. The proposed antenna has been designed and analysed using the high frequency structure simulator (HFSS).

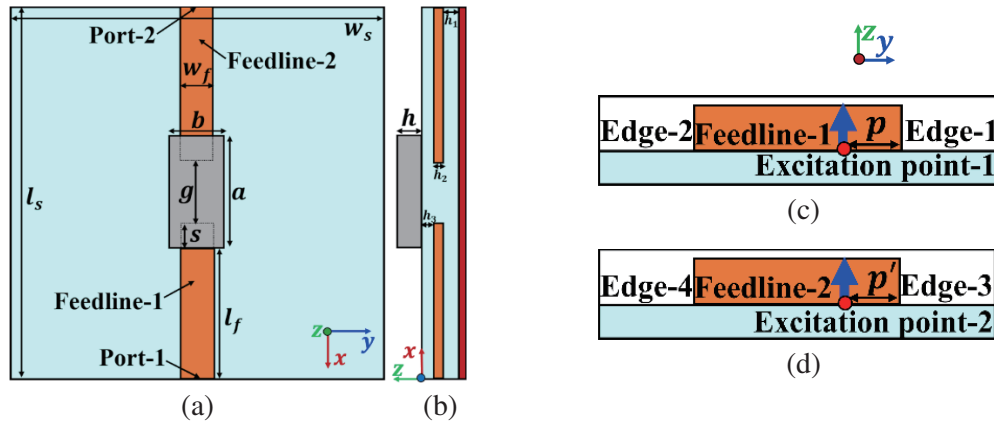


Figure 1. (a) Top view, and (b) lateral view of the proposed antenna geometry, (c) Excitation position at distance p in feedline-1 and (d) p' in feedline-2 from the corner of the edge-1 and edge-3, respectively. $l_s = w_s = 4$, $h_1 = 0.145$, $h_2 = 0.03$, $h_3 = 0.01$, $a = 1.2$, $b = 0.6$, $h = 0.325$, $l_f = 1.625$, $w_f = 0.34$, $s = 0.225$, and $g = 0.75$, (Units in μm).

3. DESIGN GUIDELINES AND ANALYSIS

The dimensions selection of the proposed rectangular DR and excitation mechanism including the feeding position have been determined by considering the optimized design guidelines. In rectangular DRA, the existence of lower order TM modes was not verified experimentally [35]. Hence, the resonant frequency of the lower order TE modes is calculated using transcendental equations reported in [36], and the characteristic equation for the wave numbers k_x , k_y , and k_z for the fundamental TE_{111}^y is well

explained in [37]. The rectangular geometry of the radiating element is the simplest one to be adopted at the miniature level with higher degree of freedom than other geometries. Mainly, the guidelines focussed on the achievement of three main outcomes which include (a) optimizing the dimensions of the DR to obtain the high aspect-ratio for the merging of fundamental and higher-order modes, (b) generating the orthogonal degenerate modes for obtaining the CP response using the specific feeding mechanism, and (c) maintaining the isolation between the ports for the MIMO operation ensuring the diversity performance. Considering these issues, the DR length and width are selected as $a = 2b$, and optimized height h is taken to maintain the high aspect ratio equivalent to $a/h \approx 2$ while splitting the DR into two equal halves ($a = b$) using the single port configuration. The high value of aspect ratio allows the excitation of the fundamental and higher order transverse electric (TE) modes [38]. For CP response, the excitation is given at the corner of the feedlines which allows the travelling wave field to achieve quarter-wavelength path difference along the edges of the respective feedlines [39]. In this manner, the width of the feedlines is taken equivalent to $w_f \approx \lambda_0/4$, where λ_0 is the operating wavelength. This path difference in the travelling field at the edges of the feedline provides 90° phase difference between the field components, which generates orthogonal modes inside the DR. This can be explained using the fundamental mathematical expression, $\phi = \frac{2\pi}{\lambda_0} \times w_f \implies \phi \approx \frac{\pi}{2}$ (for 193.5 THz resonant frequency, and $0.34 \mu\text{m}$ feedline width), where w_f is the feedline width. Further, maintaining isolation between the ports is also one of the prominent and challenging tasks [40]. A detailed study has been done in order to analyse the scope of MIMO concept in the field of antenna designing and its integration with other system [41]. Considering this, the isolation between the ports is maintained by gap, g , which is optimized using the parametric analysis in this proposed antenna. It is interesting to note that good isolation is maintained at gap, g , which separates feedline by the distance equivalent to $\approx \lambda_0/2$. Further, different feeding locations at the respective ports ensure the diversity performance with the achievement of both CP and LP responses across the overlapped frequency passband. Furthermore, an extended work can be considered on the possibility of developing a semi-analytical technique that can predict the interaction of the excitation source with the resonators of various geometries to provide a physical explanation at THz regime likewise reported in [42, 43].

4. RESULTS AND DISCUSSIONS

Figures 1(c) and (d) show the feeding arrangement of the proposed antenna. The excitation positions have been maintained using parameters p and p' at feedline-1 and -2, respectively as shown in Figs. 1(c) and (d). These excitation positions maintain the desired path difference for the achievement of LP and CP radiations. Initially, the excitation is given at the corners of the feedlines maintaining positions at $p = p' = 0$. The resultant phase difference of the field components is maintained at 90° when the field components travel with the quarter-wavelength path different along the edges of the feedlines. This allows the generation of orthogonal degenerate modes inside the DR. Thus, CP response has been obtained. However, any deviation in the path difference at excitation position disturbs the field components resulting in LP radiations at the port. For obtaining the polarization diversity, parameters p and p' have been further analysed and optimized at different positions of the ports.

For the better understanding of the proposed antenna mechanism, two different antennas have been analysed. The antenna geometries with respective feeding arrangements are shown in Figs. 2(a) and (b). Antenna-1 has feeding positions at $p = p' = 0$ which is responsible for the generation of circular polarization. However, Antenna-2 has asymmetrical feeding positions at $p = 0$ and $p' = 0.05$. Consequently, Antenna-2 provides polarization diversity resulting in the achievement of LP and CP radiations using different ports. Fig. 2(c) shows the frequency response of the real and imaginary impedances of Antenna-2. The imaginary impedance tends to zero at resonating frequencies of both the ports. This represents that the near field power is very little. Thus, the imaginary part is assumed as non-radiating in nature. Moreover, the value of real part is high, and this indicates that the combined power is either transmitted or received by the proposed antenna. The frequency response of the S -parameters using antenna-1 providing 7.8% (185–200 THz) of the operating impedance bandwidth is shown in Fig. 2(d). For brevity, the antenna-1 response using port-1 has only been plotted as $S_{11} = S_{22}$ and $S_{12} = S_{21}$ due to symmetric feeding positions. Further, the axial-ratio (AR) bandwidth of 4.04% (185.94–193.59 THz) is obtained as shown in Fig. 2(f). The specific feeding arrangement excites the

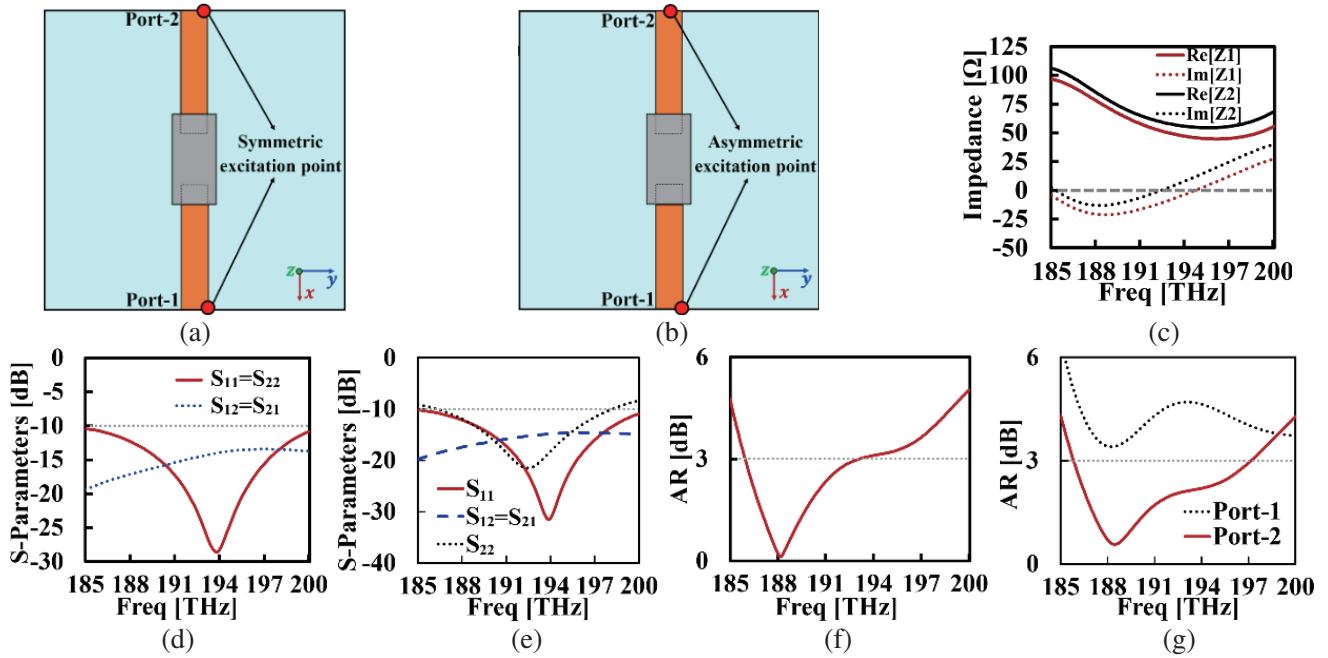


Figure 2. Feeding geometry of (a) antenna-1, (b) antenna-2, frequency response of the (c) impedance (real and imaginary), (d), (e) *S*-parameters, (f), and (g) AR of antenna-1 and antenna-2, respectively.

orthogonal degenerate mode inside the radiating element resulting in CP response. Moreover, these orthogonal modes maintain the isolation of more than 15 dB between the ports even using the single radiating element. Later, the feeding positions have been shifted to achieve the polarization diversity. In Antenna-2, the asymmetric feeding positions result in the shifting of p' at port-2 which leads to the deviation from quarter-wavelength path difference. This disturbs the phase difference between the field components travelling across the feedline which results in the LP response using port 2. However, port-1 provides CP radiations with no change in feeding position. This confirms the achievement of polarization diversity. In addition, the optimised value of p' is selected in such a manner that it will not disturb the *S*-parameter of the antenna drastically. The isolation is also maintained at the value of 15 dB or more between the ports which is acceptable for the MIMO diversity performance. Figs. 2(e) and (g) show the simulated *S*-parameter and AR response of the proposed antenna-2 with polarization diversity, respectively. This antenna provides the simulated impedance bandwidth of 7.79% (185–200 THz) and 6.17% (186.30–198.17 THz) using port-1 and port-2, respectively. The simulated 3 dB AR in the boresight direction ($\theta = 0^\circ$) provides the wide bandwidth of 6.78% (185.82–198.9 THz) using port 1. However, port-2 provides the LP response of the antenna.

Further, the radiation mechanism of the antenna can be understood by analysing the field distribution. Fig. 3 shows the *E*-field distribution inside the DR of antenna-2. The field distribution has been observed in the *yz*-plane and *xz*-plane using port-1 and -2, respectively. The field distribution at 188.3 THz resonant frequency is shown in Figs. 3(a) and (b). This field distribution resembles the TE_{111}^x and TE_{111}^y modes which confirms the existence of the orthogonal degenerate modes. The field distribution at 193.5 THz resonant frequency confirms the TE_{121}^x and TE_{211}^y modes distributions as shown in Figs. 3(c) and (d). Similarly, the field distribution at 195.2 THz resonant frequency resembles the TE_{131}^x and TE_{311}^y modes as shown in Figs. 3(e) and (f). The merging of the pair of fundamental, second and third order orthogonal degenerate modes provides a wider bandwidth. The field distribution in the constant $z = h$ plane has also been observed which confirms the 2π rotation of the field vectors with the time frame varying from 0 to T [21]. However, for brevity the rotation of the field vectors is not reported.

The radiation patterns of antenna-2 with the excitation at port-1 for the resonant frequencies 188.3 THz, 193.5 THz, and 194.7 THz in the *xz* and *yz*-plane, respectively, are shown in Figs. 4(a)–

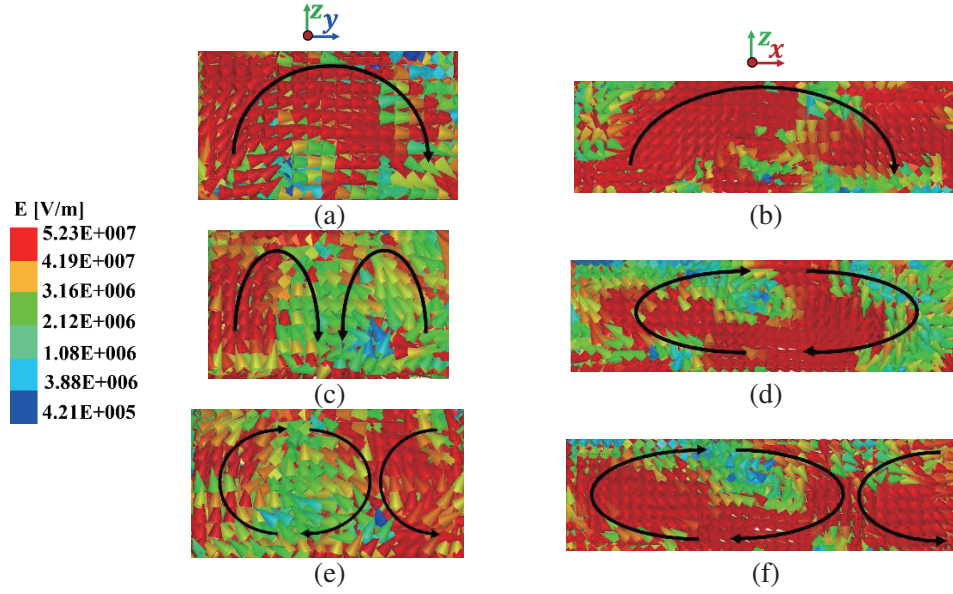


Figure 3. E -field distribution at (a) 188.3 THz, (b) 193.5 THz and (c) 195.2 THz inside the DR using excitation at port-1.

(f). The proposed antenna provides RHCP dominant radiations for the resonant frequencies. The separation between the co- and cross-polarized components remains 19 dB or more in the boresight direction ($\theta = 0^\circ$) for both xz - and yz -planes. The antenna provides the peak gain of 7.1 dBic and 6.8 dBic in the boresight direction using port-1 and port-2, respectively as shown in Fig. 4(g). Fig. 4(h) shows the simulated radiation efficiency of the antenna. It remains more than 78% across the entire operating passband of the antenna using both the ports. The performance comparison of the proposed antenna with the other reported nano-DRAs is shown in Table 1.

Table 1. Comparison of the proposed antenna with other reported nano-DRAs. (f_r : resonant frequency, BW_{im} : impedance bandwidth, BW_{AR} : axial-ratio bandwidth, P_1 : port-1 and P_2 : port-2, NR: Not reported).

Ref.	DR structure	Operating frequency (THz)	f_r (THz)	BW_{im} (%)	BW_{AR} (%)	No. of ports	Gain
[16]	Cylindrical	185–205	193.5	10.25	0	1	7.5
[17]	Hexagonal	190.9–198.1	193.5	3.7	0	1	NR
[18]	Triangular	192.5–197.3	193.5	2.58	0	1	NR
[19]	Dielectric rod	172–222	190	25.38	0	1	9
[15]	Cylindrical	187–210	193.5	11.58	5.72	1	NR
This DR	Rectangular	P_1 : 185–200	P_1 : 192.5	P_1 : 7.79	P_1 : 6.78	2	P_1 : 7.1
		P_2 : 186.3–198.2	P_2 : 193.5	P_2 : 6.17	P_2 : 0		P_2 : 6.8

5. PARAMETRIC ANALYSIS

The feeding arrangement of antenna-1 and antenna-2 has been analysed using the parametric study. The effect of the variation of p and p' from edge-1/3 of feedline-1 and 2, respectively, has been studied and analysed. In antenna 1, the optimized values of these parameters are selected as $0.34 \mu\text{m}$ for the achievement of CP radiations. However, any change in these positions results in LP radiation at the

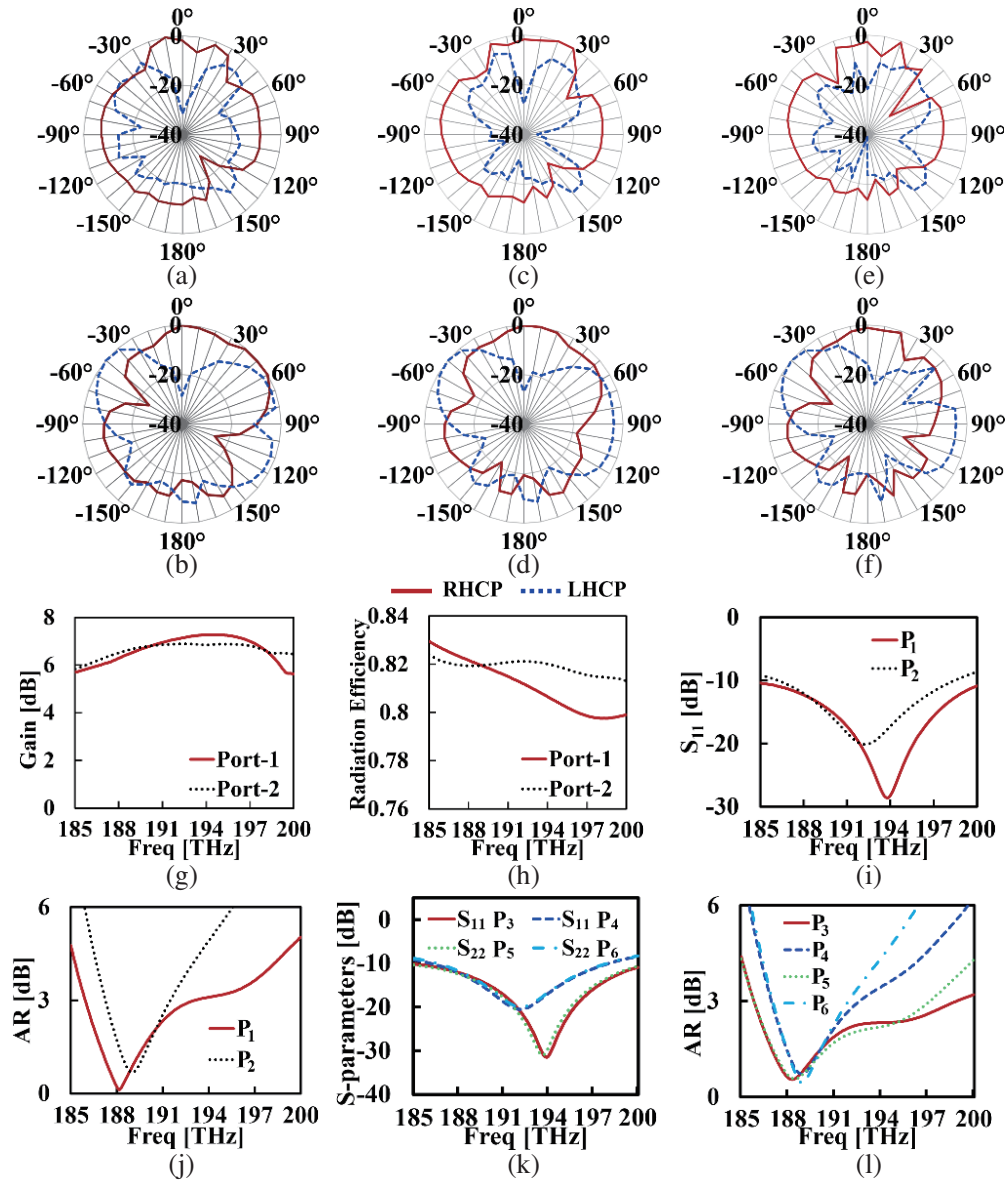


Figure 4. Radiation pattern at (a), (b) 188.3 THz, (c), (d) 193.5 THz, (e), (f) 195.2 THz using port-1 of Antenna-2 (top: radiation pattern in xz -plane and bottom: radiation pattern in yz -plane) and frequency response of (g) gain, (h) radiation efficiency, (i), (j) frequency response of S -parameters and AR response using different feeding arrangement in Antenna-1, and (k), (l) Antenna-2, respectively.

port. Similarly for antenna-2, the value of p or p' is optimised at $0.05 \mu\text{m}$ and $0.29 \mu\text{m}$. It is done with the consideration that it would not affect the S -parameters of the antenna drastically. These positions lead to the achievement of LP radiations using the respective ports. This confirms the polarisation diversity. The effect of these parameters on the frequency response of the S -parameter and 3 dB AR bandwidth has been studied in this parametric analysis. The frequency response of S_{11} parameters and AR using antenna-1 has been analysed using different feeding positions. The optimised excitation position parameters are selected as P_1 ($p = 0, p' = 0$) and P_2 ($p = 0, p' = 0.34$) for the respective cases. Figs. 4(i) and (j) show the frequency response of the antenna parameters using excitation positions as per P_1 and P_2 . It is observed that the feeding positions arrangement in P_1 provides more impedance matching with wide AR bandwidth. In addition, it is worth mentioning that the radiation

pattern confirms the dual-sense polarization of the antenna with the excitation positions according to P_1 . The antenna provides right-hand circularly polarized (RHCP) and left-hand circularly polarized (LHCP) responses using port-1 and port-2, respectively. However, P_2 provides RHCP dominant polarization using both the ports. The radiation patterns are reported for the brevity. Figs. 4(k) and (l) show the frequency response of S -parameters and AR using antenna-2. The excitation positions have been optimised using the feeding arrangement as P_3 ($p = 0, p' = 0.05$) P_4 ($p = 0, p' = 0.29$, P_5 ($p = 0.05, p' = 0$) and P_6 ($p = 0.05, p' = 0.34$). The antenna with feeding arrangement as P_3 and P_4 provides CP response at port-1 and LP response at port-2. However, P_5 and P_6 feeding arrangement provides the CP and LP radiations using port-2 and port-1, respectively, thus confirming the achievement of polarization diversity with the slight shift in the excitation positions. Consequently, these parameters are chosen in such a manner that it would not change the other antenna parameters drastically.

6. CONCLUSION

The proposed optical antenna explores the possibilities of using highly efficient DRAs over the conventional metallic antennas at THz regime. A technique has been adopted for obtaining the CP response as well as polarization diversity in the two-port MIMO nano-DRA. The antenna confirms the polarization diversity with the CP radiations using port-1 and LP radiations using port-2 with the achievement of 6.78% of AR bandwidth. Considering the preliminary stage of this proposed work, the detailed design guidelines and analysis are also discussed. Electromagnetic simulators are used for the numerical and theoretical analysis. Consequently, this field requires the development in the field of communication with the perspective of fabrication and measurement in future. This leads to the development in the field of nanotechnology by reducing the size of the nano-networks effectively. The proposed antenna with these optimized dimensions can be utilized for the optical C- and L-band applications.

FUNDING

The authors received no financial support for the research, authorship, and publication of this research work.

DISCLOSURES

The authors declare no conflicts of interest.

REFERENCES

1. Novotny, L., "Optical antennas: A new technology that can enhance light-matter interactions," *Front. Eng.*, Vol. 39, No. 4, 100–120, 2012, doi: 10.1364/AOP.1.000438.
2. Abadal, S., E. Alarcón, A. Cabellos-Aparicio, M. Lemme, and M. Nemirowsky, "Graphene-enabled wireless communication for massive multicore architectures," *IEEE Commun. Mag.*, Vol. 51, No. 11, 137–143, 2013, doi: 10.1109/MCOM.2013.6658665.
3. Pohl, D., "Near-field optics seen as an antenna problem in near-field optic," *World Sci.*, Vol. Near-Field, 9–21, 1999.
4. Mühlischlegel, P., H. J. Eisler, O. J. F. Martin, B. Hecht, and D. W. Pohl, "Applied physics: Resonant optical antennas," *Science*, Vol. 308, No. 5728, 1607–1609, 2005, doi: 10.1126/science.1111886.
5. Schuck, P. J., D. P. Fromm, A. Sundaramurthy, G. S. Kino, and W. E. Moerner, "Improving the mismatch between light and nanoscale objects with gold bowtie nanoantennas," *Phys. Rev. Lett.*, Vol. 94, No. 1, 14–17, 2005, doi: 10.1103/PhysRevLett.94.017402.
6. Huang, J.-S., T. Feichtner, P. Biagioni, and B. Hecht, "Impedance matching and emission properties of optical antennas in a nanophotonic circuit," *Nano Lett.*, Vol. 9, No. 5, 1897–1902, 2008, doi: 10.1021/nl803902t.

7. Kinzel, E. C. and X. Xu, "High efficiency excitation of plasmonic waveguides with vertically integrated resonant bowtie apertures," *Opt. Express*, Vol. 17, No. 10, 8036–45, 2009, doi: 10.1364/oe.17.008036.
8. Wen, J., S. Romanov, and U. Peschel, "Excitation of plasmonic gap waveguides by nanoantennas," *Opt. Express*, Vol. 17, No. 8, 5925–32, 2009, doi: 10.1364/oe.17.005925.
9. Schnell, M., et al., "Nanofocusing of mid-infrared energy with tapered transmission lines," *Nat. Photonics*, Vol. 5, No. 5, 283–287, 2011, doi: 10.1038/nphoton.2011.33.
10. Sethi, W. T., H. Vettikalladi, H. Fathallah, and M. Himdi, "Nantenna for standard 1550 nm optical communication systems," *Int. J. Antennas Propag.*, Vol. 2016, 1–9, 2016, doi: 10.1155/2016/5429510.
11. Novotny, L. and N. Van Hulst, "Antennas for light," *Nat. Photonics*, Vol. 5, No. 2, 83–90, 2011, doi: 10.1038/nphoton.2010.237.
12. Ulukus, S., et al., "Energy harvesting wireless communications: A review of recent advances," *IEEE J. Sel. Areas Commun.*, Vol. 33, No. 3, 360–381, 2015, doi: 10.1109/JSAC.2015.2391531.
13. Citroni, R., F. Di Paolo, and P. Livreri, "Evaluation of an optical energy harvester for SHM application," *AEU — Int. J. Electron. Commun.*, Vol. 111, 152918, 2019, doi: 10.1016/j.aeue.2019.152918.
14. Walther, M., D. G. Cooke, C. Sherstan, M. Hajar, M. R. Freeman, and F. A. Hegmann, "Terahertz conductivity of thin gold films at the metal-insulator percolation transition," *Phys. Rev. B — Condens. Matter Mater. Phys.*, Vol. 76, No. 12, 1–9, 2007, doi: 10.1103/PhysRevB.76.125408.
15. Mongia, R. K. and P. Bhartia, "Dielectric resonator antennas — a review and general design relations for resonant frequency and bandwidth," *Int. J. Microw. Millimeter — Wave Comput. Eng.*, Vol. 4, No. 3, 230–247, 1994, doi: 10.1002/mmce.4570040304.
16. Luk, K. M. and K.-W. Leung, *Dielectric Resonator Antennas*, Research Studies Press, 2003.
17. Kajfez, D., A. Elsherbeni, and A. Mokaddem, "Higher order modes in dielectric resonators," *IEEE AP-S Antennas Propagat. Symposium*, 306–309, 1996.
18. Kajfez, D., A. W. Glisson, and J. James, "Computed modal field distributions for isolated dielectric resonators," *IEEE Trans. Microw.*, Vol. 32, No. 12, 1609–1616, 1984.
19. Bolivar, P. H., et al., "Measurement of the dielectric constant and loss tangent of high dielectric-constant materials at terahertz frequencies," *IEEE Trans. Microw. Theory Tech.*, Vol. 51, No. 4I, 1062–1066, 2003, doi: 10.1109/TMTT.2003.809693.
20. Yi, H., S. W. Qu, and C. H. Chan, "Wideband dielectric resonator terahertz reflectarray," *ICCEM 2015 — 2015 IEEE International Conference on Computational Electromagnetics*, 273–274, 2015, doi: 10.1109/COMPEM.2015.7052631.
21. Varshney, G., S. Gotra, J. Kaur, V. S. Pandey, and R. S. Yaduvanshi, "Obtaining the circular polarization in a nano-dielectric resonator antenna for photonics applications," *Semicond. Sci. Technol.*, Vol. 34, No. 7, 07LT01, 2019, doi: 10.1088/1361-6641/ab1fd1.
22. Sidiropoulos, T. P. H., M. P. Nielsen, T. R. Roschuk, A. V. Zayats, S. A. Maier, and R. F. Oulton, "Compact optical antenna coupler for silicon photonics characterized by third-harmonic generation," *ACS Photonics*, Vol. 1, No. 10, 912–916, 2014, doi: 10.1021/ph5002796.
23. Maram, R., S. Kaushal, J. Azaña, and L. R. Chen, "Recent trends and advances of silicon-based integrated microwave photonics," Vol. 6, No. 1. 2019.
24. Toh, B. Y., R. Cahill, and V. F. Fusco, "Understanding and measuring circular polarization," *IEEE Trans. Educ.*, Vol. 46, No. 3, 313–318, 2003, doi: 10.1109/TE.2003.813519.
25. Valagiannopoulos, C. A., M. Mattheakis, S. N. Shirodkar, and E. Kaxiras, "Manipulating polarized light with a planar slab of black phosphorus," *J. Phys. Commun.*, Vol. 1, No. 4, 2017, doi: 10.1088/2399-6528/aa90c8.
26. Sarsen, A. and C. Valagiannopoulos, "Robust polarization twist by pairs of multilayers with tilted optical axes," *Phys. Rev. B*, Vol. 99, No. 11, 1–10, 2019, doi: 10.1103/PhysRevB.99.115304.
27. Perhirin, S. and Y. Auffret, "Circularly polarized nanoring antenna for uniform overheating applications," *Microw. Opt. Technol. Lett.*, Vol. 55, No. 11, 2562–2568, 2013, doi: 10.1002/mop.

28. Gotra, S., G. Varshney, R. S. Yaduvanshi, and V. S. Pandey, "Dual-band circular polarisation generation technique with the miniaturisation of a rectangular dielectric resonator antenna," *IET Microwaves, Antennas Propag.*, Vol. 13, No. 10, 8–14, 2019, doi: 10.1049/iet-map.2019.0030.
29. Sharawi, M. S., "Current misuses and future prospects for printed multiple-input, multiple-output antenna systems," *IEEE Antennas Propag. Mag.*, Vol. 59, No. 2, 162–170, 2017, doi: 10.1109/MAP.2017.2658346.
30. Takase, D. and T. Ohtsuki, "Optical wireless MIMO communications (OMIMO)," *GLOBECOM — IEEE Glob. Telecommun. Conf.*, Vol. 2, No. 5, 928–932, 2004, doi: 10.1109/glocom.2004.1378096.
31. Chen, Y., B. Weng, and J. Liu, "A novel photonic-based MIMO radar architecture with all channels sharing a single transceiver," *IEEE Access*, Vol. 7, 165093–165102, 2019, doi: 10.1109/ACCESS.2019.2953105.
32. Rui, G., R. L. Nelson, and Q. Zhan, "Circularly polarized unidirectional emission via a coupled plasmonic spiral antenna," *Opt. Lett.*, Vol. 36, No. 23, 4533, 2011, doi: 10.1364/ol.36.004533.
33. Ding, G., C. Clavero, D. Schweigert, and M. Le, "Thickness and microstructure effects in the optical and electrical properties of silver thin films," *AIP Adv.*, Vol. 5, No. 11, 117234–11, 2015, doi: 10.1063/1.4936637.
34. Headland, D., et al., "Terahertz magnetic mirror realized with dielectric resonator antennas," *Adv. Mater.*, Vol. 27, No. 44, 7137–7144, 2015, doi: 10.1002/adma.201503069.
35. Mongia, R. K. and A. Ittipiboon, "Theoretical and experimental investigations on rectangular dielectric resonator antennas," *IEEE Trans. Antennas Propag.*, Vol. 45, No. 9, 1348–1356, 1997, doi: 10.1080/02726343.2017.1261222.
36. Marcatili, E. A. J., "Dielectric rectangular waveguide and directional coupler for integrated optics," *Bell Syst. Tech. J.*, Vol. 48, 2071–2102, 1969, doi: 10.1002/j.1538-7305.1969.tb01166.x.
37. Gotra, S. and V. S. Pandey, "Critical analysis of the recent trends and advancements in dielectric resonator antennas," *Progress In Electromagnetics Research B*, Vol. 97, 167–197, 2022.
38. Gotra, S., G. Varshney, V. S. Pandey, and R. S. Yaduvanshi, "Super-wideband multi-input–multi-output dielectric resonator antenna," *IET Microwaves, Antennas Propag.*, Vol. 1, No. 1, 1–8, 2019, doi: 10.1049/iet-map.2018.6112.
39. Garg, R., P. Bhartia, I. Bahl, and A. Ittipiboon, *Microstrip Antenna Design Handbook*, Artech House, London, UK, 2001.
40. Hussain, N., T. D. Pham, and H.-H. Tran, "Circularly polarized MIMO antenna with wideband and high isolation characteristics for C-band communication systems," *Micromachines*, Vol. 13, No. 11, 1894, 2022, doi: 10.3390/mi13111894.
41. Prabhu, P., M. Subramani, and K. Sup Kwak, "Analysis of integrated UWB MIMO and CR antenna system using transmission line model with functional verification," *Sci. Rep.*, Vol. 12, No. 1, 1–18, 2022, doi: 10.1038/s41598-022-17550-z.
42. Moussu, M. A. C., et al., "Reply to comments on 'a semi-analytical model of high-permittivity dielectric ring resonators for magnetic resonance imaging'," *IEEE Trans. Antennas Propag.*, Vol. 70, No. 4, 3131, 2022, doi: 10.1109/TAP.2022.3143879.
43. Valagiannopoulos, C. A. and N. K. Uzunoglu, "Rigorous analysis of a metallic circular post in a rectangular waveguide with step discontinuity of sidewalls," *IEEE Trans. Microw. Theory Tech.*, Vol. 55, No. 8, 1673–1683, 2007, doi: 10.1109/TMTT.2007.901597.